CHEMBIOCHEM

DOI: 10.1002/cbic.200700465

Electrostatic Stabilization and General Base Catalysis in the Active Site of the Human Protein Disulfide Isomerase a Domain Monitored by Hydrogen Exchange

Griselda Hernández,[a] Janet S. Anderson,[b] and David M. LeMaster*[a]

*The nucleophilic Cys36 thiol of the human protein disulfide isomerase **a** domain is positioned over the N terminus of the α_2 helix. Amides in the active site exhibit diffusion-limited, hydroxide-catalyzed exchange, indicating that the local positive electrostatic potential decreases the p*K* value for peptide anion formation by at least 2 units so as to equal or exceed the acidity of water. In stark contrast to the pH dependence of exchange for simple peptides, the His38 amide in the reduced enzyme exhibits a maximum rate of exchange at pH 5 due to efficient general base catalysis by the neutral imidazole of its own side chain and suppression of its exchange by the ionization of the Cys36 thiol. Ionization of this thiol and deprotonation of the His38 side chain suppress the Cys39 amide hydroxide-catalyzed exchange by a million-fold. The electrostatic potential within the active site monitored by these exchange experiments provides a means of stabilizing the two distinct transition states that lead to substrate reduction and oxidation. Molecular modeling offers a role for the conserved Arg103 in coordinating the oxidative transition-state complex, thus providing further support for mechanisms of disulfide isomerization that utilize enzymatic catalysis at each step of the overall reaction.*

Introduction

The catalytic domains of the protein disulfide isomerases (PDI) share structural homology with other members of the thioredoxin superfamily, all of which bear an active site containing a C-X-Y-C sequence. The redox potentials among the members of this family vary by more than 150 mV, which corresponds to a difference in equilibrium constants of more than 10^5 for the two-electron transfer reaction at 25 °C. This variation in redox potentials largely arises from differences in the thiol p*K* value of the N-terminal cysteine,[1,2] which serves as the primary nucleophile that attacks the disulfide linkages of the protein substrate. As a result, the p*K* of this cysteine thiol provides an indication of whether these proteins will act predominantly as oxidants or as reductants under physiological conditions. Considerable effort in electrostatic modeling has been applied to predicting the varying p*K* values of the N-terminal cysteine among the PDIs and their thioredoxin relatives.[3–6]

More directly germane to the catalytic reactivity of these enzymes is the active-site stabilization of the linear trisulfur transition state that forms during the thiolate–disulfide exchange reaction. The majority of the negative charge density from the incoming thiolate is shared between the terminal cysteines of this S_N2 reaction complex.[7] Enzymatic catalysis could be facilitated by establishing a diffuse positive electrostatic potential within the active site to complement the diffuse negative charge density of the trisulfur complex. As illustrated in the recent X-ray structure of the PDI from *Saccharomyces cerevisiae* (PDB code: 2B5E),[8] the sulfur of the N-terminal cysteine of the **a** domain active site is positioned above the amide groups from the initial turn of the α_2-helix (Figure 1). Wada[9] first proposed that the parallel arrangement of the individual peptide dipoles would give rise to a helix macrodipole, and Hol[10]

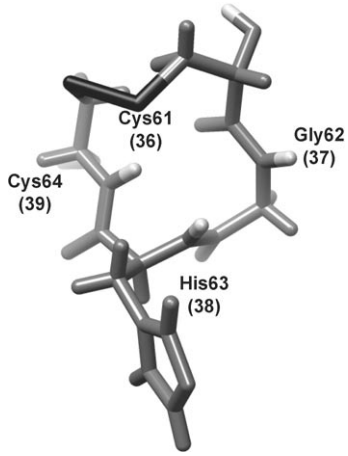

Figure 1. Active site of the **a** domain of protein disulfide isomerase from *Saccharomyces cerevisiae* in the oxidized form.[8] The first turn of the α_2 helix is shown, in which the sulfur of Cys61 (black) lies above the amide protons of Gly62, His63, and Cys64 (white). The corresponding sequence positions in the human PDI **a** domain are indicated in parentheses.

[a] *Prof. G. Hernández, Prof. D. M. LeMaster*
Wadsworth Center
New York State Department of Health and
Department of Biomedical Sciences
School of Public Health, University at Albany–SUNY
Empire State Plaza, Albany, NY 12201 (USA)
Fax: (+1) 518-473-2900
E-mail: lemaster@wadsworth.org

[b] *Prof. J. S. Anderson*
Department of Chemistry, Union College
Schenectady, NY 12308 (USA)

Supporting information for this article is available on the WWW under http://www.chembiochem.org or from the author.

argued for the role of this macrodipole in active-site catalysis. In our refinement of the *E. coli* thioredoxin X-ray structure,[11] we suggested that the linear trisulfur transition state is stabilized by the diffuse positive electrostatic potential arising from such a helix dipole.

Although the electrostatic potential at the N terminus of the α-helix is generally understood to be of positive sign, serious disagreement remains as to the magnitude and spatial extent of this potential and hence to its significance in transition-state stabilization. The physical realism of the helix macrodipole concept has been called into question.[12] Recent calculations[13] have suggested that the dielectric shielding of the solvent reaction field dramatically attenuates the magnitude of the α-helix dipole. A survey[14] of 212 aspartate and glutamate residues with measured p*K* values from known protein structures found that the acidic side chains located at the N termini of α-helices have an average p*K* value that is 0.6 units lower than for the other tertiary positions. However, it has been argued that these systematically lower carboxyl p*K* values arise predominantly from an increased density of specific hydrogen-bonding interactions in this structural region.[15] Similarly, cysteine residues at the N termini of model α-helices are found to have markedly lower p*K* values only at the so-called N-cap position (e.g., Cys61 of Figure 1), arguably due to the ability of the thiolate in this position to form hydrogen bonds with the solvent-exposed amides of the helix.[16]

To more fully characterize the magnitude and extent of the positive electrostatic field emanating from the N terminus of an α-helix, a more extensive set of experimental monitors needs to be established. Although the peptide linkage is far less acidic than the carboxyl, thiol, imidazolium, and ammonium groups of the ionizable side chains, it also acts as a normal Eigen acid[17] such that its kinetic acidity directly reflects its thermodynamic acidity. As a result, an alteration in the p*K* value for individual amide nitrogens is directly reflected in the rate of hydroxide-catalyzed amide hydrogen exchange,[18–20] so that under appropriate conditions these exchange rates can provide a sensitive monitor of the local electrostatic potential within the protein structure.[21,22]

The reaction rate of the reduced **a** domain with the non-physiological substrate bis-hydroxyethyldisulfide (the oxidized form of 2-mercaptoethanol) is nearly as fast as that for oxidized glutathione near physiological pH and substrate concentrations.[23] In contrast, under these conditions, a simple model cysteine reacts with these substrates more slowly by factors of 300- and 600-fold, respectively. The bis-hydroxyethyldisulfide substrate offers little opportunity for rate enhancement that occurs through a specific binding interaction with the residues of the **a** domain active site. On the other hand, an electrostatic interaction with the enzyme that stabilizes the negative charge of the linear trisulfur transition state by a factor of $\sim 10^2$, relative to the solution-phase reaction, could largely account for the observed catalytic acceleration.

Creighton and co-workers[24] were unable to detect the amide hydrogen resonances for the Gly37 and His38 residues that lie between the active-site cysteine residues of the oxidized human PDI **a** domain at pH 5.1. They proposed that the absence of these resonances results from an increased rate of hydrogen exchange due to the enhanced acidity of these amides resulting from the local positive electrostatic potential at the N terminus of the α_2-helix. We have detected these active-site amide resonances in both the oxidized and reduced forms of the PDI **a** domain and have determined their exchange rates in the reduced form as a function of pH.

Characterizing the structural basis of **a** domain catalysis is further complicated by the fact that there are two distinct trisulfur transition states that differ substantially in their charge distribution and their positioning within the active site. The mixed disulfide intermediate formed between Cys36 of the **a** domain and a cysteine of the substrate can break down via either of two pathways. When the solvent inaccessible Cys39 side chain attacks the mixed disulfide intermediate, the Cys36 sulfur becomes the central atom of the linear trisulfur transition state that leads to substrate reduction. Substrate oxidation arises from the attack of a thiolate from the protein substrate on the mixed disulfide intermediate. In this case, Cys36 contributes a terminal sulfur in the transition state.

Formally, disulfide isomerization can be achieved by two (or more) steps of disulfide reduction followed by two (or more) steps of reoxidation in which a differing disulfide linkage pattern is generated. However, despite over 40 years of study,[25] the physiologically relevant mechanism of the overall isomerase reaction remains a topic of debate. In the absence of a redox buffer, Gilbert and co-workers[26] showed that the unscrambling of an oxidized protein substrate by PDI is sensitive to the levels of both the oxidized and reduced forms of the enzyme; this is consistent with isomerization via a reduction–reoxidation cycle. On the other hand, more recently Raines and colleagues[27] utilized kinetic data obtained from a novel homogenous substrate to argue for the alternative mechanism of intramolecular isomerization (Scheme 1). In marked contrast to

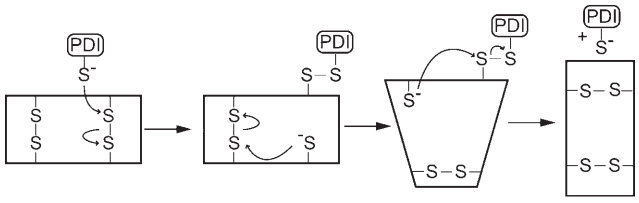

Scheme 1. Intramolecular isomerization mechanism. The cysteine thiolate of PDI attacks a disulfide linkage of the substrate protein. Following disulfide rearrangement within the substrate, the mixed disulfide linkage with PDI is cleaved to generate the second substrate disulfide.

the reduction–reoxidation mechanism in which every step of the reaction is catalyzed by the enzyme, the central step of the intramolecular isomerization pathway is the uncatalyzed reaction between a cysteine thiolate and a disulfide linkage within the substrate protein. Clarification of how the **a** domain stabilizes both transition states will help to address the plausibility of an overall disulfide isomerization mechanism in which each reaction step is enzymatically catalyzed.

Results and Discussion

Hydrogen exchange in the active site of the PDI a domain

To test the hypothesis of Creighton and co-workers[24] that rapid hydrogen exchange accounts for the absence of $^{1}H,^{15}N$ crosspeaks for the Gly37 and His38 active-site residues in the oxidized human PDI **a** domain, we carried out analogous measurements utilizing the FHSQC NMR pulse sequence.[28] By minimizing the saturation of the solvent $^{1}H_2O$ resonance, this pulse sequence decreases the loss of signal amplitude arising from chemical-exchange dynamics. At pH 5.0, the Gly37 amide resonance was observed. Lowering the pH to 4.0 yielded the His38 resonance as well. The identification of these two resonances was established by HNCA[31,32] through-bond correlations and NOESY through-space correlations to the known resonances of the Cys39 residue[24] (see the Supporting Information). Similarly, a weak His38 crosspeak was observed for the reduced form of the enzyme at pH 4 and was used to establish the resonance assignments across the active-site sequence (Figure 2).

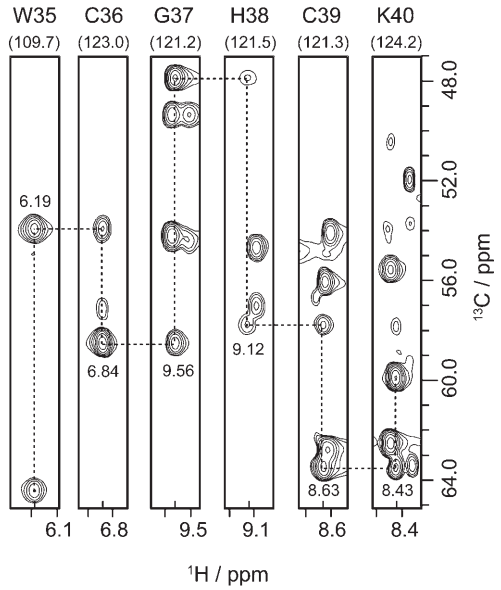

Figure 2. 3D HNCA correlation spectra showing connectivities across the active-site sequence of the reduced human PDI **a** domain at pH 4.0. The amide ^{1}H chemical shifts are indicated within each spectral strip, while the ^{15}N chemical shifts are given in parentheses below the residue names. Referencing of the ^{15}N chemical shifts to the ^{1}H carrier frequency[29] yields values that differ by −1.9 ppm from the previously published assignments of the oxidized protein.[30]

Rapid hydrogen exchange kinetics can be measured by using a magnetization transfer-based experiment, such as CLEANEX-PM,[33] in which magnetization from the solvent $^{1}H_2O$ resonance is allowed to chemically exchange into the amide ^{1}H resonances, which are then observed. These experiments confer increased sensitivity for the detection of severely broadened resonances near the fast-exchange limit. At pH 4.0, both Gly37 and His38 of the oxidized **a** domain yielded $^{1}H,^{15}N$ amide crosspeaks in a CLEANEX-PM spectrum (Figure 3 A). A reference experiment[34] serves to enhance the accuracy of the exchange-rate measurements by facilitating correction for the spin relax-

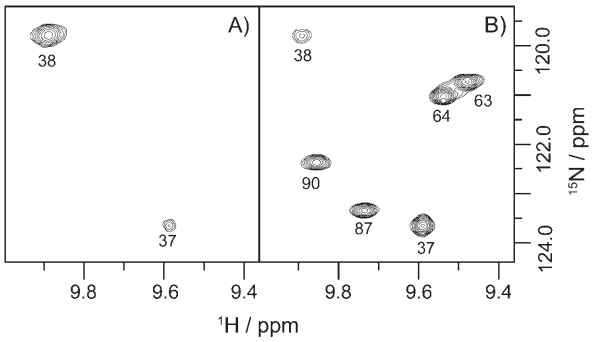

Figure 3. 2D $^{1}H,^{15}N$ CLEANEX-PM and reference HSQC spectra of the oxidized **a** domain of human PDI at pH 4.0. A) The CLEANEX-PM experiment,[33,34] which monitors the transfer of magnetization from the bulk water resonance to the amide protons, exhibits signals for Gly37 and His38 at this low pH value. B) Due to substantial exchange broadening, the reference HSQC peak for the His38 amide is markedly weaker than the peaks for other nearby resonances.

ation that occurs during the CLEANEX-PM mixing time (Figure 3 B). Under these conditions, the amide of His38 exchanges at a rate of 60 s^{-1}, 400-fold faster than the rate for the corresponding model dipeptide.[35]

In Figure 4, pairs of CLEANEX-PM (above) and reference (below) spectra for the reduced **a** domain are illustrated for pH values ranging from 3.98 to 10.05. The amide of Asp1 exhibits rapid hydroxide-catalyzed exchange at pH 3.98 due to the adjacent positively charged terminus of the initial methionine residue, which is not removed during expression of this gene in *E. coli*. As the pH is raised, the CLEANEX-PM crosspeak of Asp1 initially increases in intensity, then broadens, and finally weakens beyond observation above pH 6.46 in a pattern consistent with the exchange rates predicted for the corresponding model dipeptide.[35] The pattern of crosspeaks for the Gly37 amide also indicates a monotonically increasing exchange rate as the pH is increased, although the increase in rate is less than proportional to the hydroxide ion concentration.

In marked contrast, the intensity of the exchange crosspeak for Cys39 is nearly constant across the entire pH range of stability for this enzyme, exhibiting an increase only as pH 10 is approached. Even more exceptional is the pH dependence of the His38 amide resonance. The broad exchange peak observed at pH 3.98 becomes significantly weaker as the pH increases toward 5, while the corresponding resonance in the reference spectra decreases to below detection. As the pH increases further, the His38 crosspeak in the reference spectra reappears and gains a substantial intensity, while the exchange peak strengthens and narrows with increasing pH; this is indicative of a decreasing rate of hydrogen exchange. Hence, the His38 amide in the active site of the PDI **a** domain exhibits a maximal exchange rate near pH 5. This stands in direct opposition to the behavior of model peptides for which the transition

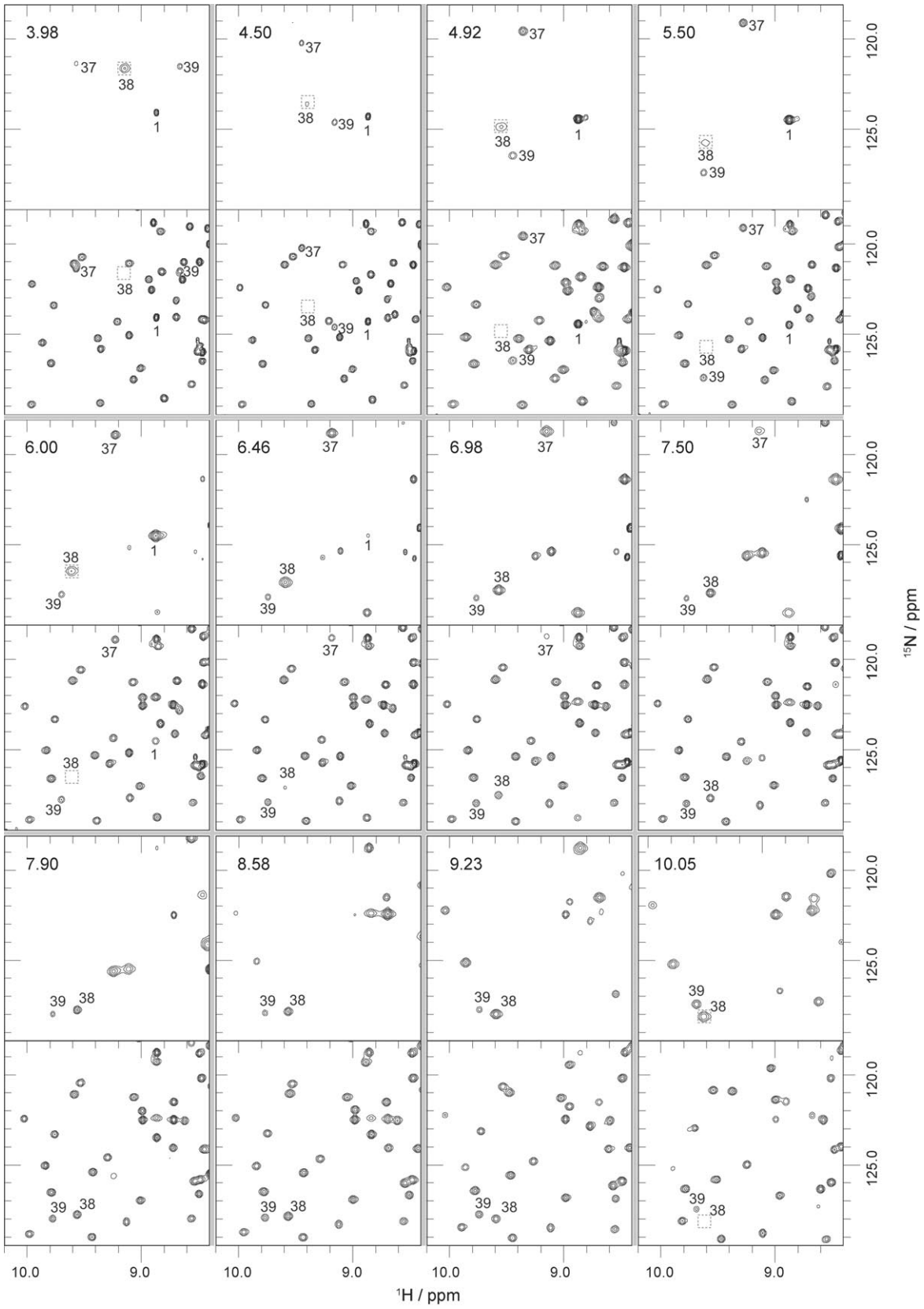

Figure 4. pH dependence of amide exchange in the reduced form of the human PDI **a** domain. Corresponding pairs of CLEANEX-PM (above) and reference (below) spectra are illustrated for pH values spanning the range of 3.98 to 10.05. In marked contrast to all other protein resonances, the CLEANEX-PM peaks for His38 and Cys39 remain observable over the entire pH range. His38 crosspeaks that are not observable in the reference spectra at the contour level displayed are indicated by dotted squares. At the pH values of 4.92 and 5.50, the His38 crosspeak is not clearly discernible above the noise level in the reference spectra.

from hydronium-ion-catalyzed to hydroxide-ion-catalyzed kinetics results in an exchange-rate minimum near pH 4. As pH 10 is approached, the exchange rate of His38 again begins to increase. Given the peculiarity of this exchange behavior for His38, the identities of the active site amides were again verified by through-bond correlation experiments at pH 6.98.

Chemical-shift titration analysis of active-site ionization

Quantitative interpretation of these hydrogen-exchange data depends upon the ionization behavior of the side chains in the active site. Creighton and co-workers determined a p*K* of 4.5 for the Cys36 thiol and a p*K* value of 6.2 ± 0.1 for the imidazole side chain of His38 for the reduced human **a** domain in 200 mM KCl.[36] To gain insight into the electrostatic coupling between these two ionizable side chains, they also reported a p*K* of 5.4 ± 0.1 for the His38 side chain in the oxidized enzyme. Assuming that the electrostatic properties of the oxidized protein mimic those of the reduced protein species in which the Cys36 side chain is neutral, they estimated a coupling interaction between the two charged side chains of 0.8 pH units; this implies a 4.6 kJ mol^{-1} interaction energy at room temperature.

As Creighton and co-workers reported a substantial ionic strength dependence for the Cys36 thiol ionization,[36] we analyzed amide NMR chemical-shift titration behavior at the 0.1 M ionic strength utilized in the hydrogen-exchange measurements (Figure 5). The ^{15}N resonances of Cys36 and Gly37 undergo large chemical-shift migrations in opposite directions that correlate with the antiparallel orientations of the two ^{1}H–^{15}N bond vectors relative to the Cys36 sulfur atom (Figure 1); this is consistent with an electrostatic-induction effect on the ^{15}N chemical shifts. Acid denaturation precludes NMR spectral analysis below pH 4, so only a portion of the titration curve was observed. Chemical-shift titration measurements were also carried out with the H38A variant of the **a** domain to determine a Cys36 thiol p*K* value of 5.41 (Figure 5). Assuming that the full range of chemical-shift migration for these two amide nitrogens is the same for the wild-type enzyme, a p*K* of 4.22 is estimated for the Cys36 thiol (Figure 5). If the H38A variant is treated as a mimic of the reduced PDI enzyme bearing an uncharged His38 side chain, the 1.19 pH unit difference in the Cys36 p*K* values between the reduced and the H38A variant predicts a 6.7 kJ mol^{-1} electrostatic coupling between the Cys36 and His38 side chains, a value 50% larger than that inferred by Creighton and co-workers[36] from the histidine titration of the oxidized and reduced enzymes.

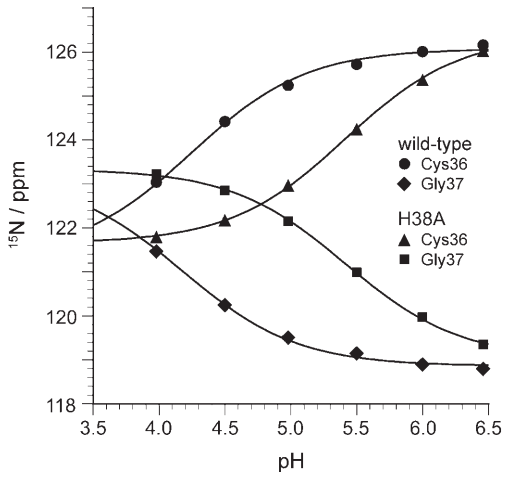

Figure 5. ^{15}N chemical-shift titration of Cys36 and Gly37 amides in the wild-type and in the H38A variant of the human PDI **a** domain in the reduced state. For both residues, the fit to the titration curves of the H38A variant yields a p*K* value of 5.41. By assuming that the full migration range for the ^{15}N chemical shifts applies equally to the wild-type enzyme, a p*K* value of 4.22 is obtained.

The active site of the PDI **a** domain also contains the ionizable thiol of the solvent-inaccessible Cys39 residue for which an unambiguous p*K* determination has not been obtained. The ^{1}H and ^{15}N shifts of Ala33 and Cys39 exhibit no significant changes over the pH range of 7 to 10. As these amide protons are located only 3.3 and 3.1 Å, respectively, from the sulfur of the solvent-inaccessible active-site cysteine in the X-ray structure of the yeast enzyme,[8] the p*K* of the Cys39 thiol in the human **a** domain would appear to be above 10. The structurally analogous buried cysteine in *E. coli* thioredoxin has an elevated p*K* value of 11.1 when the solvent-exposed cysteine thiol is alkylated to provide a stable covalent mimic of the enzyme–substrate mixed-disulfide intermediate.[37] A comparably elevated p*K* value for the structurally buried Cys39 of the **a** domain is potentially consistent with the carboxyl side chain of Glu30 serving as a general acid/base catalyst for (*de*)protonation of the Cys39 thiol, as has been demonstrated for the structurally homologous Cys35 and Asp26 residues of *E. coli* thioredoxin.[38]

Hydroxide-catalyzed exchange in the a domain active site

The amide exchange rates for residues Asp1, Gly37, His38, and Cys39 of the reduced enzyme are plotted as a function of pH in Figure 6. The exchange rates of Asp1 agree closely with the rates predicted from model peptide values,[35,39] as expected for the structurally disordered N terminus of the **a** domain.[30] The exchange kinetics of Gly37 exhibit a markedly slower rate of increase as a function of pH. When the rate is plotted on a logarithmic scale, the hydroxide dependence of the Gly37 amide exchange has a slope of only 0.4, as opposed to the value of 1.0 anticipated for a simple hydroxide-catalyzed reaction. As illustrated in Figure 1, the amide nitrogen of Gly37 is 4 Å from the Cys36 sulfur and 5 Å from the His38 side chain. The conversion of the Cys36 thiol to the thiolate form and the His38 imidazolium to the neutral imidazole form as the pH increases yields a less positive local electrostatic potential. As a result, the peptide anion intermediate that is formed during the hydroxide-catalyzed exchange reaction of the Gly37 amide will be increasingly destabilized, yielding a weakened dependence of exchange rate on pH.

As the pH increases above 3.98, the exchange rate of Cys39 H^N remains near 5.2 s^{-1} up to pH 6.0. Above this pH, the rate modestly decreases by 25% (Figure 6). The near pH independence of these exchange rates across a million-fold variation in

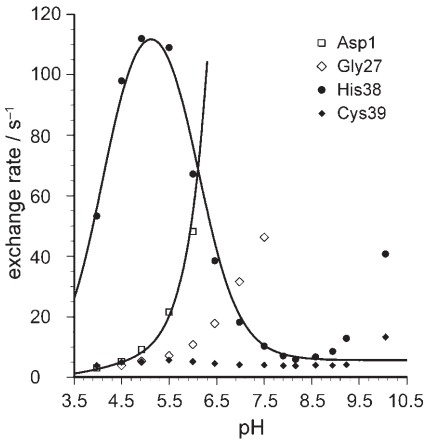

Figure 6. pH dependence of amide exchange rates for Asp1 and the active site of the human **a** domain of PDI. Model peptide exchange rates,[35,39] calculated for the N-terminal Met–Asp dipeptide by assuming a side-chain carboxyl p*K* of 4.0, closely match the observed exchange rates for Asp1 (□). The amide of Gly37 (◇) exhibits a much weaker pH dependence, while the exchange of Cys39 (◆) is nearly pH independent up to almost pH 10. Under the assumption that hydroxide-catalyzed hydrogen exchange only occurs when the Cys36 sulfur is uncharged, the exchange data of His38 (●) were fitted to the estimated population of the imidazolium ($Cys^{\circ}His^{+}$) and neutral imidazole ($Cys^{\circ}His^{\circ}$) forms of His38, assuming macroscopic p*K* values of 4.22 and 6.0 for Cys36 and His38, respectively, and a 4.6 kJ mol^{-1} electrostatic coupling interaction to derive the microscopic ionization constants.[40,41]

hydroxide ion concentration spans the full range of pH for which the stability of this protein permits such exchange measurements. Although pH-independent exchange rates are commonly interpreted to indicate that conformational access of a given amide hydrogen to the bulk solvent is rate-limiting (i.e., the EX1 kinetic limit),[42] at pH 4 the model peptide rate for this amide is 0.15 s^{-1},[35,39] approximately 25-fold slower than the observed rate. Hence, the protein tertiary structure gives rise to an acceleration rather than a retardation of the hydrogen exchange.

An alternate interpretation proposes that ionization of the nearby Cys36 thiol strongly suppresses the formation of the Cys39 peptide anion, so that, over the pH range from 4 to nearly 10, exchange will occur only from the fraction of the protein for which the Cys36 side chain is in the neutral thiol form. As the pH increases above the cysteine p*K* value of 4.22, the fraction of neutral thiol species decreases in approximately inverse proportion to the increasing hydroxide ion concentration. Since the product of the neutral thiol concentration and the hydroxide ion concentration will be nearly constant, the predicted exchange rates are essentially pH independent. In this interpretation, the 25% decrease in the exchange rates that occurs near pH 6 for the Cys39 amide would arise from the deprotonation of the His38 side chain and the resultant decrease in the electrostatic stabilization of the peptide anion intermediate. The rise in the exchange rate for the Cys39 amide near pH 10 is consistent with the onset of significant hydroxide-catalyzed exchange for the Cys36 thiolate protein species. However, since denaturation becomes significant above pH 10 for the human PDI **a** domain, destabilization of the protein structure might also contribute to the observed increase in exchange rate.

Even though the pH dependence of the exchange behavior of His38 appears more complex than that of Cys39 (Figure 6), the data can be fitted under the same assumption that the Cys36 thiolate strongly suppresses the ionization of the His38 amide. The Cys36 thiol p*K* value of 4.2 determined herein, the reported p*K* value of 6.2 for the His38 imidazole,[36] and the electrostatic coupling between these two side chains allow the microscopic ionization constants for the $Cys^{\circ}His^{+}$, $Cys^{\circ}His^{\circ}$, $Cys^{-}His^{+}$, and $Cys^{-}His^{\circ}$ species to be calculated.[40,41] Assuming that the last two species do not significantly contribute to exchange, the exchange rate constants for the $Cys^{\circ}His^{+}$ and $Cys^{\circ}His^{\circ}$ forms can be optimized to fit the observed exchange data for His38 (Figure 6). The fit to the experimental data is markedly improved by adjustment of the macroscopic p*K* value for the His38 side chain to 6.0. However, the quality of the fit is rather insensitive to the assumption of whether the electrostatic coupling interaction energy between the Cys36 thiolate and the His38 imidazolium groups is 4.6[36] or 6.7 kJ mol^{-1}. Hence, the analysis given herein is largely unaffected by which of these two estimates for the inter-side-chain interaction energy is more accurate. On the other hand, the present data do not provide a clear basis for discriminating between these two values for the electrostatic coupling.

Based on the analysis illustrated in Figure 6, the fraction of the reduced enzyme predicted to be in the $Cys^{\circ}His^{+}$ form at pH 4 is 0.58; this implies an apparent hydroxide-catalyzed exchange rate constant of His38 in the $Cys^{\circ}His^{+}$ form of 1.0×10^{12} M^{-1} s^{-1}. This apparent rate constant is a 100-fold above the diffusion limit. As such a prediction appears to be physically implausible, an alternate mechanism must be considered.

General base catalysis in the a domain active site

Simple model peptides undergo hydroxide-catalyzed exchange with rate constants of $\sim10^{8}$ M^{-1} s^{-1}, roughly 100-fold more slowly than a diffusion-limited reaction.[35] These kinetics reflect the fact that the p*K* of the peptide nitrogen is approximately two units higher than that of water (p*K* of 15.7).[18] The acidity of an amide can be modulated by introducing electron-withdrawing groups into the R substituent for a series of *N*-methylamides $RCONHCH_3$.[18–20] As the amide acidity increases, the hydroxide-catalyzed rate constant increases until the diffusion limit of 2×10^{10} M^{-1} s^{-1} at 25 °C in 0.1 M ionic strength is reached (conditions also utilized in the present study).

At pH 4, the amides of Asp1, Gly37 and Cys39 in the reduced **a** domain all have exchange rates that are in the range of 2 to 3 s^{-1}. As [OH^{-}] is equal to 10^{-10} M at pH 4, in each case the diffusion-limited, hydroxide-catalyzed rate has been reached. For Asp1, the substituent effects from the adjacent positively charged N-terminal ammonium group and the side-chain carboxyl group predict a 200-fold acceleration in hydroxide-catalyzed exchange, relative to the rate for an alanine dipeptide.[35] In similar fashion, the structural environment of Gly37 and Cys39 serve to lower the p*K* values for these peptide

groups so that their acidities are greater than or equal to that of water.

For each redox state in the H38A variant of the **a** domain, both Gly37 and Ala38 exhibit exchange rates near 1.0 s^{-1} at pH 4 (Table 1). In each case, the exchange rate increases with pH, consistent with an hydroxide-catalyzed reaction. These rates closely approach the diffusion limit, indicating that the p*K* values for these active site amides have decreased by at least ~2 units so that their acidities are equal to or greater than that of water.

Table 1. Amide hydrogen-exchange rates [s^{-1}] of the PDI **a** domain at pH 4.0.

	Gly37	His/Ala38
wild-type$_{red}$	2.9	54
wild-type$_{ox}$	2.8	60
H38A$_{red}$	1.6	1.4
H38A$_{ox}$	0.8	1.0

Simple model peptides exchange almost exclusively by either hydronium or hydroxide ion catalysis due to the fact that both protonation and deprotonation of the peptide unit are less favorable than the analogous reactions for the water molecule. Even at the pH value at which the exchange rate is at a minimum, neutral water-catalyzed exchange accounts for only ~$^1/_4$ of the observed rate.[35] The increased acidity of the amides in the active site of the **a** domain implies that weaker bases can more effectively compete with the hydroxide ion for catalysis of the hydrogen-exchange reaction, analogous to the general base catalysis reported for the series of acidic *N*-methylamides.[19,20] General base catalysis offers a mechanism that explains the dramatically accelerated exchange rate of His38 in the wild-type **a** domain at pH 4.

For the reduced form of the wild-type **a** domain, the two groups within the active site that might act as general bases are the thiolate of Cys36 and the neutral imidazole of His38 (Scheme 2). Since the exchange rate of the His38 amide at pH 4 is similar in both the oxidized and reduced forms of the enzyme (Table 1), the Cys36 thiolate does not appear to contribute significantly to the observed exchange. On the other hand, the plausibility of general base catalysis by the neutral imidazole of His38 is supported by the fact that the fraction of the reduced enzyme predicted to be in the Cys°His° form at pH 4 in Figure 6 is very similar to the fraction of neutral imidazole that is predicted at this pH for the oxidized enzyme with a p*K* value of 5.4 for the His38 side chain.[36] Given that the geometry of interaction of the imidazole side chain with the His38 amide is expected to be similar in the two redox states, having essentially the same fraction of the species that is active as a general base is fully consistent with the similar rate of exchange for this amide that is observed at pH 4 for the oxidized and reduced enzymes. In contrast to the reduced enzyme, as the pH is increased with the oxidized **a** domain, no subsequent decrease in hydrogen exchange rate is expected, since inhibition of exchange due to the ionization of the Cys36 thiol cannot occur.

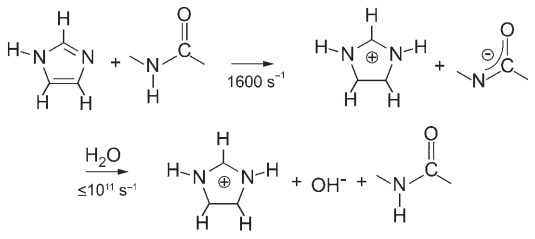

Scheme 2. General base catalysis of the His38 amide by its neutral imidazole side chain. Given macroscopic p*K* values of 4.2 and 6.0 for the Cys36 thiol and the His38 side chain, respectively, and a 4.6 kJ mol^{-1} electrostatic coupling between them, the imidazole-catalyzed hydrogen exchange is predicted to occur at a rate of 1600 s^{-1}. Reprotonation of the peptide by water will occur at a rate of ~10^{11} s^{-1} if the amide p*K* is equal to or above the p*K* of water, and will be proportionally slower for a more acidic amide.

As noted in the previous section, the bell-shaped profile for the pH dependence of exchange for the His38 amide in Figure 6 is consistent in form with the Cys°His^+ species of the enzyme facilitating the hydroxide-catalyzed reaction through a favorable electrostatic interaction with the peptide anion intermediate. However, since [Cys°His^+]·[OH^-] is directly proportional to [Cys°His°], the fit to the experimental exchange data of Figure 6 cannot distinguish between the hydroxide-catalyzed and the neutral imidazole-catalyzed mechanisms. Near pH 8.5 the amides of His38 and Cys39 exchange with similar rates. These kinetics are consistent with a pH-dependent change in mechanism such that both amides exchange through an hydroxide-catalyzed reaction of the Cys°His° form of the enzyme under these conditions, in which the higher concentration of hydroxide ion can effectively compete with the neutral imidazole catalysis. The apparent absence of general base catalysis of hydrogen exchange for the amide of Cys39 might reflect the fact that the histidine side chain cannot adopt a low-energy, hydrogen-bonding geometry with this amide without altering the conformation of other residues in the X-ray structure.[8]

The efficiency of general base catalysis is commonly expressed in terms of the corresponding rate of the reaction catalyzed by neutral water. Corrected to 25 °C, the water-catalyzed exchange rate for poly-D,L-alanine is ~0.05 min^{-1}.[35,39] Although only limited data are available on substituent effects for the water-catalyzed hydrogen exchange of simple peptides, use of the hydroxide correction factors for the neighboring side chains has been recommended.[35] For the neutral His38 form, this represents a rate correction of only 15%. The 1600 s^{-1} rate for the neutral imidazole catalysis of the His38 amide exchange reaction, estimated from the microscopic ionization constants for a 4.6 kJ mol^{-1} electrostatic coupling, is accelerated beyond the neutral-water-catalyzed reaction rate by a factor of 2×10^6.

Molecular modeling of the PDI a domain transition states

The hydrogen-exchange data for the H38A variant of the human **a** domain demonstrate that the amides of Gly37 and Ala38 exhibit hydroxide-catalyzed rates that are nearly equal to the diffusion limit; this indicates that the interactions with the surrounding tertiary structure have lowered the p*K* values for these amides to near that of water. Although the role of longer-range electrostatic interactions with other charged side chains of the enzyme cannot be excluded by the present data, the positive electrostatic potential that arises from the orientation of the peptide units within the α_2-helix would appear to be predominantly responsible for the increased acidities of the amides within the active site.

With this experimental evidence for a diffuse positive electrostatic potential within the active site of the human **a** domain, consideration may be given to how the relatively diffuse negative-charge distribution of the linear trisulfur transition states can be stabilized. The X-ray structure of the homologous **a** domain from yeast[8] was used for molecular modeling. The absence of resonances for the Gly37 and His38 amides contribute to a less well defined active-site region in the solution structure of the human **a** domain.[30] The conformation of the Arg103 side chain, discussed below, was not constrained by NOE connectivities in the original solution structure, although more recent solution structures of an homologous mouse **a** domain (PDB ID: 2DJ1, unpublished data) and an homologous human **a**′ domain (PDB code 1X5C, unpublished data) indicate positioning of this Arg side chain similar to that found in the X-ray structure of the yeast enzyme.[8]

The linear trisulfur complex formed in the substrate reduction reaction, subsequently referred to as the inner transition state, can be straightforwardly defined by the in-line attack of a thiolate from the substrate on the disulfide bond of the oxidized PDI domain (Figure 7 A). To generate this model (the homologous human residues are listed in parentheses), only the side chains of Cys61 (Cys36), Cys64 (Cys39), and His63 (His38) were allowed to readjust. The positively charged side chain of His63 is readily positioned so as to coordinate the partial negative charge of the terminal sulfur atom from the substrate. The histidine side chain is likewise well positioned to accept a proton from the incoming thiol and to donate a proton back to the thiolate leaving group. The terminal methyl group representing the cysteine C^{β} of the protein substrate is oriented toward the hydrophobic cleft formed by the side chain of Trp60 (Trp35) on one face and the backbone of Gly104 (Gly81) and the side chain of Phe105 (Tyr82) on the other face. The C-terminal fragment of the Ref-1 peptide that is covalently attached via a stabilized mixed disulfide to human thioredoxin binds in this hydrophobic cleft.[43] Modeling of the outer transition state formed during the substrate oxidation reaction is less straightforward. The intermolecular disulfide bond in the covalent complex of the Ref-1 peptide with human thioredoxin is oriented approximately perpendicular to the active-site disulfide in the oxidized enzyme. The bond vector of the mixed disulfide points toward the highly conserved active-site *cis*-Pro106 (Pro83), so that the attacking thiolate is anticipated to approach from that general direction. Lying approximately along this line in the yeast PDI **a** domain is the guanidinium group of Arg126 (Arg103). This arginine is conserved not only in PDI **a** domains from yeast to mammals, but also among many of the human PDI homologues.[44] Ruddock and co-workers[45] have shown that mutation of this arginine to a glutamine in the human **a** domain results in a fourfold decrease in the rate of oxidation of a model dithiol-containing peptide. If the enzyme is to efficiently catalyze the formation of the outer transition state, a stabilizing interaction with the $\sim{}^1/_2\,e^-$ charge on the outermost sulfur of the complex is anticipated. This arginine side chain can offer such an interaction. In analyzing the X-ray structures of the redox states of the structurally homologous dsbA, Martin and colleagues[46] noted that reduction of the enzyme results in a subtle readjustment of the backbone of the active site C–P–H–C segment, so as to permit hydrogen bonding between the amide of the histidine residue and the thiolate sulfur. A similar conformational transition would help to stabilize the $\sim{}^1/_2\,e^-$ charge on this sulfur atom that forms the second terminal position in the linear trisulfur outer transition state.

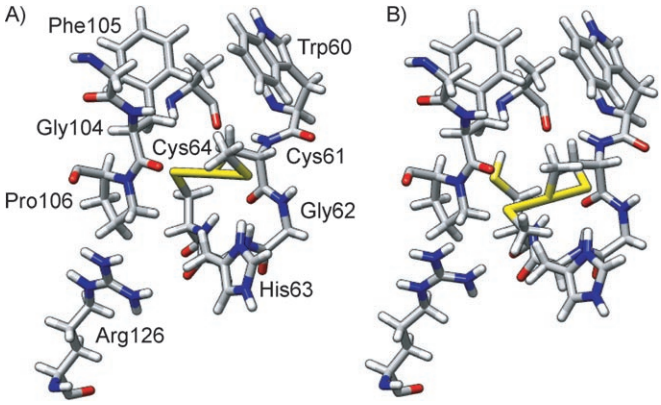

Figure 7. Model structures of the inner and outer trisulfur transition states of the yeast PDI **a** domain. A) A model of the linear trisulfur S_N2 transition state arising from attack of the solvent-inaccessible active-site cysteine on the mixed-disulfide intermediate formed between the **a** domain and the substrate. The terminal methyl, representing the cysteine of the substrate, projects toward the hydrophobic groove bounded by the indole ring of Trp60, the phenyl ring of Phe105, and the backbone of Gly104. B) A model of the outer transition state arising from the attack of a cysteine from the protein substrate on the mixed disulfide intermediate. The guanidinium group of Arg126 was modestly readjusted so as to enhance its interaction with the partial negative charge located on the terminal sulfur of the complex.

A model for the outer transition state was generated that accommodates the described characteristics by orienting the trisulfur complex between the side chains of His63 and Pro106 and then carrying out energy minimization in which only the atoms between the carbonyl carbon of Trp60 and the C^{α} of Cys64 are permitted to move (Figure 7 B). A hydrogen-bonding potential was then applied between the $H^{\eta 1}$ and $H^{\eta 2}$ atoms of Arg126 and the terminal sulfur of the transition state. The methyl group representing the substrate cysteine C^{β} that contributes the central atom of the outer trisulfur transition state is oriented in a similar fashion as in the inner transition state model, while the terminal methyl group projects toward the

orientation adopted by the N-terminal fragment of the Ref-1 peptide in the mixed disulfide complex with human thioredoxin,[43] potentially enabling analogous noncovalent interactions between the enzyme and substrate.

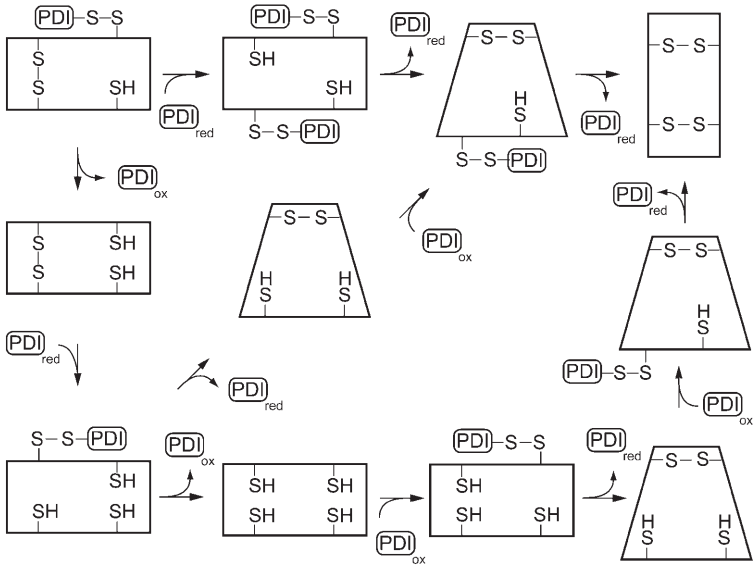

Scheme 3. Protein disulfide isomerization utilizing only enzymatically catalyzed transitions. Disulfide exchange by mixed disulfide isomerization is illustrated across the top line of the scheme. The counter-clockwise pathway depicts the reduction–reoxidation mechanism. Branching diagonally from the lower left hand corner is illustrated a combined reduction–mixed disulfide isomerization–reoxidation pathway that eliminates one step of reduction–reoxidation, while at the same time removing the assumption of concurrent mixed-disulfide complexes that characterizes the mixed-disulfide isomerization mechanism.

Mechanisms of disulfide isomerization

The intramolecular isomerization model (Scheme 1) assumes that the mixed disulfide that is formed between PDI and the protein substrate remains intact until completion of the uncatalyzed disulfide rearrangement within the substrate protein.[27] Measurements by Gilbert and co-workers[26] provide an estimate of the kinetic stability for this mixed disulfide. In the absence of oxidized glutathione, they determined that concentrations of reduced glutathione above 0.5 mM are required in order to appreciably shift the fraction of reduced PDI from the steady-state values seen at lower glutathione concentrations during the unscrambling of oxidized RNase A. Since both the **a** and **a**′ domains of PDI react with reduced glutathione with rate constants near 200 $M^{-1} s^{-1}$,[23] the average rate at which PDI releases the RNase A substrate to form the oxidized enzyme is of the order of 1 s^{-1}, which is comparable to the reactivity seen with simple glutathione substrates. This comparatively rapid attack upon the mixed disulfide by the buried cysteine is believed to provide an "escape" mechanism for the elimination of catalytically unproductive intermediates.[47,48]

As illustrated by the example of bovine pancreatic trypsin inhibitor, uncatalyzed disulfide rearrangements can have lifetimes of as long as two weeks.[49] The disparity in timeframe between such uncatalyzed disulfide rearrangements and cleavage of the mixed disulfide between the enzyme and substrate can be artificially altered by mutation of the solvent-inaccessible cysteine in the active site of PDI. However, such a mutant enzyme only catalyzes disulfide isomerization of the substrate protein in the presence of a redox buffer that can serve to cleave and regenerate the mixed disulfide between the enzyme and the protein substrate.[47]

Reaction mechanisms that utilize only enzyme-catalyzed transitions are illustrated in Scheme 3. Across the top of this scheme is given the mixed-disulfide isomerization pathway. This pathway presents a potential kinetic inefficiency in that the initially formed mixed disulfide must remain intact until after the second mixed disulfide has formed. Although the pair of active sites in PDI offers a mechanism to enhance the rate of formation of the second mixed disulfide, concurrent utilization of the two active sites would imply a degree of cooperativity that has not been observed in mutational studies.[47]

The reduction–reoxidation pathway is illustrated along the counter-clockwise loop of Scheme 3. At three intermediate steps in this pathway, the substrate is not covalently bound to the enzyme, so dissociation of the complex can occur. Utilizing particularly the **b**′ domain,[50] the peptide binding capacity of PDI can function to suppress premature dissociation of the substrate. As indicated by the diagonal pathway, the fully reduced state might be kinetically redundant, since the two mixed-disulfide states that it connects are formally equivalent. A reduction mixed-disulfide isomerization–reoxidation pathway avoids the primary limitation of the simple mixed-disulfide isomerization pathway, in that only one mixed disulfide between PDI and the substrate need be present at any given time. In addition, by eliminating the fully reduced substrate protein as an intermediate, the unproductive dissociation of this noncovalently bound species is avoided. Clearly, partially reduced protein substrates that are generated by other enzymes or by direct reactions between the substrate and glutathione can be readily incorporated at the corresponding position within this overall scheme. At the same time, the catalytic role of PDI is surely not limited to the transition-state-stabilization effects considered in this study. Often significant conformational transitions must occur in order to establish the appropriate spatial positioning for a pair of cysteines to yield disulfide formation, and the peptide binding characteristics of PDI can facilitate the diffusional component of this process.

Conclusions

The positioning of the human PDI **a** domain active site at the N terminus of the α_2-helix shifts the p*K* values for the amides in that segment so that their acidities are equal to or greater than that for water in both the oxidized and reduced forms of the wild-type and H38A variant enzymes. The positive electrostatic potential necessary to cause this increase in amide acidity is of a similar magnitude to that required to explain the cat-

alytic acceleration of glutathione and bis-hydroxyethyldisulfide reduction through electrostatic stabilization of the transition state.

This increase in thermodynamic acidity of the amides within the active site, in turn, renders the His38 amide susceptible to general base catalysis by the neutral imidazole side chain of His38, which is a million-fold more efficient than general base catalysis by the bulk solvent. We believe this to be the first example of general base catalysis of amide hydrogen exchange demonstrated within a protein. The active-site histidine and arginine side chains and the dipolar interactions of the α_2-helix contribute to a diffuse positive electrostatic potential that can serve to stabilize both the inner and outer linear trisulfur transition states. By facilitating the substrate disulfide oxidation reactions that occur via the outer transition state, the interactions of this arginine can contribute to the kinetic efficiency of protein disulfide isomerization pathways that utilize exclusively enzymatically catalyzed transitions.

Although the enhancement of amide acidity in the **a** domain active site is seemingly adventitious to the mechanism of disulfide isomerization, Brennan and Clarke[51] have shown that the rate of asparagine degradation via a succinimide intermediate is dependent on the acidity of the backbone amide nitrogen. The resultant formation of isoaspartate residues is a major source of spontaneous protein damage under physiological conditions.[52] On the other hand, nature utilizes the anion formed from the side-chain amide of asparagine to generate the essential N-glycosylation linkages in proteins[53] and to cleave the protein chain at the C-terminal junction of self-splicing intein systems.[54] The hydrogen-exchange data of the **a** domain illustrate how local tertiary interactions can facilitate the generation of the amide anion species that serves as the primary nucleophile in these biological reactions.

Experimental Section

Protein expression and purification: The gene sequence for the human PDI **a** domain was chemically synthesized (Genscript, Piscataway, NJ) with codon optimization for expression in *Escherichia coli*. The gene was cloned into the pET3a plasmid by utilizing the NdeI and BamH1 restriction sites. Site-directed mutagenesis was carried out according to the vendor protocols (Stratagene). The expression plasmids were transformed into the BL21(DE3) *E. coli* strain (Novagen, La Jolla, CA). The expression and purification of the **a** domain were carried out according to a protocol similar to that previously described,[55] with the exception that the phenyl Sepharose column of the earlier protocol was replaced with a Sephadex G-75 gel filtration column equilibrated in the Tris buffer (20 mM) used for the subsequent Q-Sepharose ion-exchange step. Oxidation of the enzyme was carried out by incubation with bis-hydroxyethyldisulfide at neutral pH.

NMR measurements: Samples of ^{15}N- and ^{13}C,^{15}N-enriched human PDI **a** domain were exchanged and concentrated by centrifugal filtration into buffers containing 7% D_2O and acetate, phosphate, or borate (20 mM) with sodium chloride added to a final ionic strength of 0.1 M. For the reduced protein samples, dithiothreitol (5 mM) was initially added to the samples and was then maintained at this concentration throughout data collection. 3D HNCA[31,32] resonance-assignment experiments were carried out on doubly labeled samples for both the oxidized and reduced **a** domains. Independent confirmation was obtained from 3D ^{1}H,^{15}N,^{1}H NOESY spectra collected with a mixing time of 60 ms. Clean chemical-exchange-phase-modulated (CLEANEX-PM)[33] spectra were collected for the ^{15}N-enriched samples as a function of pH with mixing times of 5.35, 10.7, and 21.4 ms. For the hard-pulse reference experiment,[34] the initial e-PHOGSY[56] component is replaced with a high-power 90° pulse. The intensities of the fully relaxed spectra were determined by exponential extrapolation of the intensities from the hard-pulse reference experiment by using three different relaxation delays. Water saturation was determined as originally proposed,[33] by measurement of the water resonance intensity after the e-PHOGSY component following steady-state cycling through the full sequence. Analogous measurements were also carried out for the hard-pulse reference experiment. The comparative intensities of the CLEANEX-PM and reference spectra were used to derive hydrogen exchange rates up to 60 s^{-1}. For more rapidly exchanging resonances in the CLEANEX-PM spectra, the differential hydrogen exchange rates Δk_{ex} were determined from the differential ^{1}H line broadening according to $\Delta k_{ex} = \pi \Delta \nu_{1/2}$ where $\nu_{1/2}$ is the line width in Hz at half-height.

Enzymatic transition-state modeling: Residues 28 to 146 of the yeast PDI X-ray structure[8] (PDB code: 2B5E) were used to represent the **a** domain. The initial positions of the thiol sulfurs from Cys61 and Cys64 were taken from the coordinates for the reduced form (20% occupancy). Hydrogens were added by using WHAT-IF[57] with hydrogen-bonding optimization. The program Chimera[58] was used to add missing atoms at the N and C termini, to generate the protonated form of His63, and to adjust the dihedral angles of the side chains of Cys61 and His63. For the transition-state complexes, S–S and S–CH_3 bond lengths were adjusted to 2.50 Å and 1.81 Å, respectively, and the C^β–S–S bond angle around the central sulfur and all C–S–S–C dihedral angles were adjusted to 90°; this is consistent with the quantum-mechanical modeling.[7] To maximize compatibility with the standard AMBER[59] atomic charge set, the charges for the central cysteine in the transition set were set to those for cystine. The atomic charges for the terminal cysteines were set to the average of the AMBER charge value set for cystine and the cysteine thiolate, so as to yield a net −0.5 e charge on each terminal residue. For the methyl groups representing the terminal substrate cysteines, the charges on the sulfur, carbon, and hydrogens were scaled proportionately to the differences between the cystine and cysteine thiolate charges to yield a net charge of −0.5 e for the residue. For the central sulfur of the outer transition state, atomic charges of −0.1844, −0.0949, and 0.0931 were used for S, C^β, and H^β, respectively. Restrained energy minimization was performed by using AMBER with the Generalized Born model 5 for solvent simulation with a cutoff of 16 Å.

For the inner transition state, the third sulfur was added in-line with the bond between the sulfurs of Cys61 and Cys64. Only the side-chain atoms of Cys61, His62, and Cys64 were allowed to move in a single round of energy minimization with a hydrogen bonding potential maintained between the His62 $H^{\delta 1}$ and the terminal sulfur. For the outer transition state, three minimization rounds were performed. In the first round, the χ_1 dihedral angle of Cys61 was rotated so as to direct the linear trisulfur group between the C^β of His63 and the pyrrolidine ring of Pro106. The C^β-S–S angle was artificially increased to 143° to remove poor van der Waals contacts. Energy minimization was carried out with only the atoms between Trp60 C and Cys64 C^α allowed to move. Hydrogen bond constraints were applied from Cys64 H^N and His63 H^N to Cys61 S. A second round of minimization was applied over the same set of

atoms with a bond-angle restraint applied for the Cys61 C^{β}–S–S angle. In the third minimization round, only the side-chain atoms of Cys61, His63, and Arg126 were allowed to move, while hydrogen bond constraints were applied between His63 $H^{\delta 2}$ to Cys61 S and between Arg126 $H^{\eta 1}$ and $H^{\eta 2}$ and the terminal sulfur of the transition-state complex. Coordinates for this model of the outer trisulfur transition state complex and the heavy atoms of the yeast PDI **a** domain that have been shifted from their positions in the X-ray structure are available as Supporting Information.

Acknowledgements

We acknowledge the use of the Wadsworth Center NMR facility and the DNA Sequencing Core as well as the technical assistance of Lynn McNaughton and Jianzhong Tang. This work was funded in part by NIH grant GM57266 (D.M.L.).

Keywords: enzyme catalysis · general base · hydrogen exchange · isomerases · NMR spectroscopy

[1] U. Grauschopf, J. R. Winther, P. Korber, T. Zander, P. Dallinger, J. C. A. Bardwell, *Cell* **1995**, *83*, 947–955.
[2] M. Huber-Wunderlich, R. Glockshuber, *Folding Des.* **1998**, *3*, 161–171.
[3] J. Warwicker, P. J. Gane, *FEBS Lett.* **1996**, *385*, 105–108.
[4] V. Dillet, H. J. Dyson, D. Bashford, *Biochemistry* **1998**, *37*, 10298–10306.
[5] E. Moutevelis, J. Warwicker, *Protein Sci.* **2004**, *13*, 2744–2752.
[6] A. T. Carvalho, P. A. Fernandes, M. J. Ramos, *J. Comput. Chem.* **2006**, *27*, 966–975.
[7] P. A. Fernandes, M. J. Ramos, *Chem. Eur. J.* **2004**, *10*, 257–266.
[8] G. Tian, S. Xiang, R. Noiva, W. J. Lennarz, H. Schindelin, *Cell* **2006**, *124*, 61–73.
[9] A. Wada, *Adv. Biophys.* **1976**, *9*, 1–13.
[10] W. G. J. Hol, *Prog. Biophys. Mol. Biol.* **1985**, *45*, 149–195.
[11] S. Katti, D. M. LeMaster, H. Eklund, *J. Mol. Biol.* **1990**, *212*, 167–184.
[12] J. Aqvist, H. Luecke, F. A. Quiocho, A. Warshel, *Proc. Natl. Acad. Sci. USA* **1991**, *88*, 2026–2030.
[13] D. Sengupta, R. N. Behera, J. C. Smith, G. M. Ullmann, *Structure* **2005**, *13*, 849–855.
[14] W. R. Forsyth, J. M. Antosiewicz, A. D. Robertson, *Proteins* **2002**, *48*, 388–403.
[15] M. A. Porter, J. R. Hall, J. C. Locke, J. H. Jensen, P. A. Molina, *Proteins Struct. Funct. Bioinf.* **2006**, *63*, 621–635.
[16] J. J. Miranda, *Protein Sci.* **2003**, *12*, 73–81.
[17] M. Eigen, *Angew. Chem.* **1963**, *75*, 489–508; *Angew. Chem. Int. Ed. Engl.* **1964**, *3*, 1–72.
[18] R. S. Molday, R. G. Kallen, *J. Am. Chem. Soc.* **1972**, *94*, 6739–6745.
[19] W. H. Wang, C. C. Cheng, *Bull. Chem. Soc. Jpn.* **1994**, *67*, 1054–1057.
[20] W. H. Wang, C. C. Cheng, *Bull. Chem. Soc. Jpn.* **1995**, *68*, 2767–2767.
[21] D. M. LeMaster, J. S. Anderson, G. Hernández, *Biochemistry* **2006**, *45*, 9956–9963.
[22] D. M. LeMaster, J. S. Anderson, G. Hernández, *Biophys. Chem.* **2007**, *129*, 43–48.
[23] N. J. Darby, T. E. Creighton, *Biochemistry* **1995**, *34*, 16770–16780.
[24] J. Kemmink, N. J. Darby, K. Dijkstra, R. M. Scheek, T. E. Creighton, *Protein Sci.* **1995**, *4*, 2587–2593.
[25] R. F. Goldberger, C. J. Epstein, C. B. Anfinsen, *J. Biol. Chem.* **1963**, *238*, 628–635.
[26] M. Schwaller, B. Wilkinson, H. F. Gilbert, *J. Biol. Chem.* **2003**, *278*, 7154–7159.
[27] E. A. Kersteen, S. R. Barrows, R. T. Raines, *Biochemistry* **2005**, *44*, 12168–12178.
[28] S. Mori, C. Abeygunawardana, M. O. Johnson, P. C. M. Vanzijl, *J. Magn. Reson. Ser. B* **1995**, *108*, 94–98.
[29] D. S. Wishart, C. G. Bigam, J. Yao, F. Abildgaard, H. J. Dyson, E. Oldfield, J. L. Markley, B. D. Sykes, *J. Biomol. NMR* **1995**, *6*, 135–140.
[30] J. Kemmink, N. J. Darby, K. Dijkstra, M. Nilges, T. E. Creighton, *Biochemistry* **1996**, *35*, 7684–7691.
[31] S. Grzesiek, A. Bax, *J. Magn. Reson.* **1992**, *96*, 432–440.
[32] L. E. Kay, G. Y. Xu, T. Yamazaki, *J. Magn. Reson. Ser. A* **1994**, *109*, 129–133.
[33] T. L. Hwang, P. C. M. vanZijl, S. Mori, *J. Biomol. NMR* **1998**, *11*, 221–226.
[34] G. Hernández, D. M. LeMaster, *Magn. Reson. Chem.* **2003**, *41*, 699–702.
[35] Y. W. Bai, J. S. Milne, L. Mayne, S. W. Englander, *Proteins Struct. Funct. Genet.* **1993**, *17*, 75–86.
[36] T. Kortemme, N. J. Darby, T. E. Creighton, *Biochemistry* **1996**, *35*, 14503–14511.
[37] D. M. LeMaster, *Biochemistry* **1996**, *35*, 14876–14881.
[38] D. M. LeMaster, P. A. Springer, C. J. Unkefer, *J. Biol. Chem.* **1997**, *272*, 29998–30001.
[39] G. P. Connelly, Y. W. Bai, M. F. Jeng, S. W. Englander, *Proteins* **1993**, *17*, 87–92.
[40] J. T. Edsall, R. B. Martin, B. A. Hollingsworth, *Proc. Natl. Acad. Sci. USA* **1958**, *44*, 505–518.
[41] D. L. Rabenstein, T. L. Sayer, *Anal. Chem.* **1976**, *48*, 1141–1146.
[42] A. Hvidt, S. O. Nielsen, *Adv. Protein Chem.* **1966**, *21*, 287–386.
[43] J. Qin, G. M. Clore, W. P. Kennedy, J. Kuszewski, A. M. Gronenborn, *Structure* **1996**, *4*, 613–620.
[44] L. Ellgaard, L. W. Ruddock, *EMBO Rep.* **2005**, *6*, 28–32.
[45] A. K. Lappi, M. F. Lensink, H. I. Alanen, K. E. H. Salo, M. Lobell, A. H. Juffer, L. W. Ruddock, *J. Mol. Biol.* **2004**, *335*, 283–295.
[46] L. W. Guddat, J. C. A. Bardwell, J. L. Martin, *Structure* **1998**, *6*, 757–767.
[47] K. W. Walker, M. M. Lyles, H. F. Gilbert, *Biochemistry* **1996**, *35*, 1972–1980.
[48] K. W. Walker, H. F. Gilbert, *J. Biol. Chem.* **1997**, *272*, 8845–8848.
[49] J. S. Weissman, P. S. Kim, *Nature* **1993**, *365*, 185–188.
[50] P. Klappa, L. W. Ruddock, N. J. Darby, R. B. Freedman, *EMBO J.* **1998**, *17*, 927–935.
[51] T. V. Brennan, S. Clarke, *Int. J. Pept. Protein Res.* **1995**, *45*, 547–553.
[52] T. Shimizu, Y. Matsuoka, T. Shirasawa, *Biol. Pharm. Bull.* **2005**, *28*, 1590–1596.
[53] R. S. Clark, S. Banerjee, J. K. Coward, *J. Org. Chem.* **1990**, *55*, 6275–6285.
[54] H. Paulus, *Annu. Rev. Biochem.* **2000**, *69*, 447–496.
[55] N. J. Darby, T. E. Creighton, *Biochemistry* **1995**, *34*, 11725–11735.
[56] C. Dalvit, G. Bovermann, K. Memmert, M. Zurini, *J. Magn. Reson.* **1992**, *96*, 174–180.
[57] J. E. Nielsen, G. Vriend, *Proteins* **2001**, *43*, 403–412.
[58] E. F. Pettersen, T. D. Goddard, C. C. Huang, G. S. Couch, D. M. Greenblatt, E. C. Meng, T. E. Ferrin, *J. Comput. Chem.* **2004**, *25*, 1605–1612.
[59] D. A. Case, I. T. E. Cheatham, T. Darden, H. Gohlke, K. M. M. R. Luo, Jr., A. Onufriev, C. Simmerling, B. Wang, R. Woods, *J. Comput. Chem.* **2005**, *26*, 1668–1688.

Received: August 9, 2007
Published online on February 26, 2008

